Copyright © 2005 American Scientific Publishers
All rights reserved
Printed in the United States of America

Journal of
Nanoscience and Nanotechnology
Vol. 5, 1768–1784, 2005

REVIEW

One-Dimensional Semiconductor Nanostructures as Absorber Layers in Solar Cells

K. P. Jayadevan[1] and T. Y. Tseng[1,2,*]

[1] *Department of Electronics Engineering and Institute of Electronics, National Chiao-Tung University, Hsinchu 300, Taiwan, Republic of China*
[2] *Department of Materials and Mineral Resources Engineering, National Taipei University of Technology, Taipei 106, Taiwan, Republic of China*

The one-dimensional (1-D) nanostructures of cadmium chalcogenides (II-VI: CdSe, CdTe), InP and GaAs (III-V), and the ternary chalcopyrites $CuInS_2$, $CuInSe_2$, and $CuInTe_2$ (I-III-VI_2) are the candidate semiconductors of interest as absorber layers in solar cells. In the confinement regime (~1–10 nm) of these 1-D nanostructures, the electronic energy levels are quantized so that the oscillator strength and the resultant absorption of solar energy are enhanced. Moreover, the discrete energy levels effectively separate the electrons and holes at the two electrodes or at the interfaces with a polymer in a hybrid structure, so that an oriented and 1-D nanostructured absorber layer is expected to improve the conversion efficiency of solar cells. The intrinsic anisotropy of II-VI and I-III-VI_2 crystal lattices and the progress in various growth processes are assessed to derive suitable morphological features of these 1-D semiconductor nanostructures. The present status of research in nanorod-based solar cells is reviewed and possible routes are identified to improve the performance of nanorod-based solar cells. Finally, the characteristics of nanorod-based solar cells are compared with the dye-sensitized and organic solar cells.

Keywords: Solar Cell, Semiconductor, Absorber Layer, Anisotropic Lattice, Vapor Phase Growth, Template-Assisted Synthesis, Solution Growth, Excitons, Hybrid Polymer/Nanostructure, Charge Transfer, Power Conversion Efficiency, Dye-Sensitized Structure, Organic Photovoltaics.

CONTENTS

1. INTRODUCTION

The search for alternative energy sources has been gathering momentum in the recent years as part of an effort to protect the environment and preserve the natural resources. One of the major threats to the environment is the burning of the fossil fuels that leads to carbon dioxide (CO_2) emission. The alarming increase in the levels of CO_2 in the atmosphere would lead to disastrous consequences that include global warming, melting of polar ice, disruption of ecosystem, weird weather patterns with drought and flooding becoming usual phenomena, rise in the sea levels and what not. The debate on alternative energy sources that exploit solar power has been of great relevance with media acting as a bridge between science and technology and common man to improve the living standards and induce an awareness about the challenges that mankind will have

*Author to whom correspondence should be addressed.

1533-4880/2005/5/1768/017 doi:10.1166/jnn.2005.445

to encounter in the coming years. Rapidly depleting natural resources has been termed as one of the major challenges that mankind faces with an ever increasing rate of consumption.[1]

The performance of a solar cell is assessed by its ability to convert the incident solar energy to consumable form of electrical energy. A conversion efficiency of ~25% has been achieved for Si-based solar cells.[2] The major hurdle for the widespread use of solar cells has been the cost associated with the processing of silicon (Si) solar cells. To overcome the high processing costs, the novel attempts are directed to find a solution from the nanoscience and nanotechnology. The low cost nanocrystalline TiO_2-based solar cells (Grätzel cells)[3] have the advantage of high surface area of nanocrystalline TiO_2 as the semiconductor layer that is sensitized with a dye. Under a suitable potential gradient, the electrons that are transferred from the activated dye to the conduction band of the semiconductor flows to a redox couple in association with an electrolyte to complete the current. This photoelectrochemical cell exhibited a conversion efficiency of 7 to 8% in simulated solar light and 12% in diffuse daylight. Alternatively, the nanocrystalline semiconductor can be deposited over a conducting substrate to function as an active solar energy absorbing layer in a usual *p-n* junction solar cell design.[4] Under illumination, an electrical current is generated when the electrodes are connected externally. The disadvantage of these types of cells has been the tunneling of electrons between the adjacent nanocrystals that impedes the free electron flow between the electrodes and hence reduces the light-to-current conversion efficiency. An apparent solution to this issue would be to use one-dimensional (1-D) semiconductor nanostructures forming channels for current flow between the electrodes. Among the nanostructured materials, 1-D nanostructures have been unique and attractive in their morphology with a high aspect ratio, charge carrier confinement and consequently, the interesting transport properties.[5] These exciting features have caught the attention of the researchers to exploit the electronic transport properties of 1-D semiconductors to improve the conversion efficiency of solar cells. Significant interest has been generated recently with the report of the design of a CdSe-based polymer/semiconductor hybrid solar cell.[6] The study demonstrated that by tuning the diameter of the CdSe nanorods, the band gap of the CdSe could be varied so as to achieve an optimum overlap between the absorption spectrum of the photovoltaic device and the solar emission spectrum. Moreover, the higher the aspect

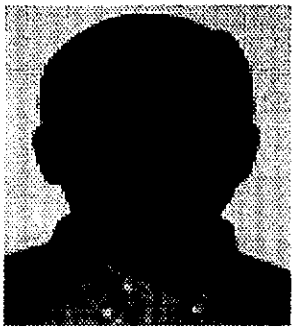

Dr. K. P. Jayadevan received his B.S. degree in Physics and his M.S. degree in Chemistry from the University of Mysore, India in 1991 and 1993, respectively. He earned his Ph.D. degree in Materials Science under the guidance of Professor K. T. Jacob from the Department of Metallurgy, Indian Institute of Science, Bangalore, India in 2000. From February 2001 to July 2005, he was working as a post-doctoral fellow with Prof. T. Y. Tseng at the Department of Electronics Engineering and Institute of Electronics of National Chiao-Tung University, Hsinchu, Taiwan. His research areas include semiconducting oxide thin films and nanomaterials. Currently, he is working as a Chemistry lecturer in an Engineering College in Bangalore, India. Dr. Jayadevan has published more than 20 research papers in scientific journals.

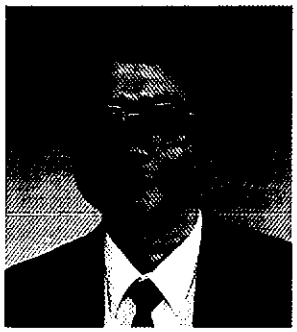

T. Y. Tseng received the Ph.D. degree in electroceramics from the School of Materials Engineering, Purdue University, West Lafayette, IN, in January 1982. Chair professor R. W. Vest was his major professor. After working at University of Florida, Dr. Tseng became a faculty member at the National Chiao-Tung University, Taiwan in 1983, the Director of the Institute of Electronics and he is now a Chair Professor in the Department of Electronics Engineering and the Institute of Electronics and also a Chair Professor of Department of Materials and Mineral Resources Engineering and Dean of College of Engineering of National Taipei University of Technology. He established Electronic Materials Research Lab and High Temperature Superconductor thin Film Lab at the Institute. His current research interests are in electronic ceramics, nanomaterials and nanodevices, passive components, high-k gate dielectrics, ferroelectric thin films and devices and electronic ceramic thin films and devices. He has published more than 210 SCI journal papers, 70 conference papers and several patents. An IEEE and ACerS Fellow, Dr. Tseng is a reviewer for a number of scientific journals, Member of Editorial Board of Journal of Nanoscience and Nanotechnology, Member of Board of Asia Ferroelectrics Association and National Science Council Distinguished Research Fellow. He has received the Distinguished Research Awards of the National Science Council (1995–2000), the Distinguished Electrical Engineering Professor Award of Chinese Electrical Engineering Society (2000), the Hou Chin-Tui Distinguished Honor Award (2002), and the Sun Yat-Sen Academic Award (2003), TECO Award (2004) and IEEE CPMT "Exceptional Technical Achievement Award" (2005) for his major contributions to the applied technology and basic science in electronic ceramics.

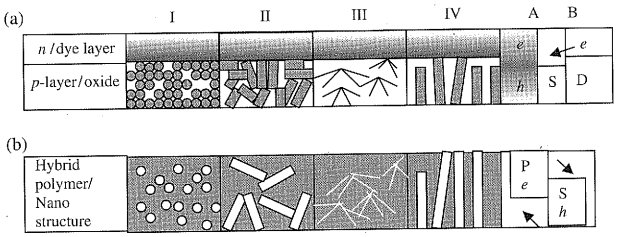

Fig. 1. Schematic diagram for nanostructures for solar cells (a) Nanostructure-based *p-n* junction/dye-sensitized structure: The upper shaded portion is *n*-type window layer or dye layer for the nanoparticle (I), randomly oriented nanorods (II), tetrapods (III), and oriented nanorod (IV)-based configurations. The *e-h* separation that leads to generation of current under illumination for a *p-n* junction (A) or the electron transfer in dye-sensitized solar cell (B) are indicated, (b) Hybrid polymer (P)/semiconductor (S) structure with the similar nanostructures as in the (a). The energy level diagram and the electron (hole) transfer process are indicated in the last panel.

ratio of the CdSe nanorods, the more efficient the electron transport between the electrodes. If these 1-D nanostructures are vertically grown over a substrate with a controlled number density as in a hybrid cell structure where a polymer separates individual nanorods,[7] then possibly higher conversion efficiency could be achieved.

A schematic diagram in Figure 1 illustrates the possible nanostructural morphologies that can be exploited for the design of solar cells. The three types of solar cells are the *p-n* junction device, dye-sensitized structure and a hybrid structure in which the donor-type polymer phase embeds the electron-accepting semiconductor phase. The mechanism of electron transport is briefly indicated in the figure. In a *p-n* junction device, while under illumination, the *n*-type semiconducting transparent window permits the passage of solar radiation to the *p*-type absorber layer. The absorber layer is characterized by a band gap that matches the incident solar energy (e.g., Air Mass (AM) 1.5 Global solar radiation for hybrid solar cells).[6] For a bulk microcrystalline solar active layer, the efficient absorption of the solar radiation is hampered by the scattering along the grain boundaries and other microdefects such as dislocations. Hence, a thickness of the order of micrometers is required for the bulk active layer for solar energy absorption. When a nanocrystalline semiconductor that is characterized by large surface-to-volume ratio is used, the scattering due to the microdefects is reduced in the absence of well defined grain boundaries and dislocations. Furthermore, the size-effect forces the electron energy levels to discrete states, which in turn leads to efficient absorption of solar radiation. Consequently, a thickness of about 200 nm would lead to efficient absorption of solar radiation in nanocrystalline semiconductor-based solar cells.[8] However, the conversion efficiency of nanocrystalline solar cells is still far less than the Si-based conventional solar cells because of the electron hopping mechanism between the adjacent nanocrystals[9] that leads to less efficient charge transport between the electrodes. In all the three types of configurations that are schematically illustrated in Figures 1(a) and (b), the electron transport through the semiconductor layer is decisive in the cell performance. Therefore, the search for efficient and low cost solar cells may be directed to finding a suitable morphology for the nanostructured layer that can form channels for electron transport. The characterization of solar cells based on nanorods of CdSe[6] and CdTe[7] indicates that the dimensional confinement enhances the charge separation, electron transport, and optical absorption of the solar cells. The tetrapod morphology (morphology III in Fig. 1) of CdSe, which may be considered as a three-dimensional (3-D) nanostructure that is generated out of 1-D CdSe nanorods, has been identified as a better morphology than 1-D CdSe nanorods for electron transport.[10] The research on 1-D nanostructure-based solar cells is still at its infancy and further investigations on materials, growth processes, and characterization are required to make a cheap and efficient solar cell that can replace expensive Si solar cells. In this short review, we examine the II-VI, III-V, and I-III-VI_2 compound semiconductors as absorber layers in solar cells based on their crystal structures, various growth processes to derive suitable morphological features for the 1-D nanostructures, and the present status of research in nanorod-based solar cells. Possible routes that could improve the performance of the nanorod-based solar cells are pointed out wherever relevant in the following discussion. The review ends with a comparison of nanorod-based solar cells with dye-sensitized and organic solar cells.

2. MATERIALS AND CRYSTAL STRUCTURES

The indirect band gap of Si, the need for its high purity, and the complicated processing steps to design Si solar cells have forced researchers to look for cheaper alternatives. Compound semiconductors that have direct band gap, high optical absorption coefficient, and tunable electronic properties may be the suitable candidates for Si replacement (e.g., CdTe with a band gap of 1.5 eV at room temperature is a good absorber of solar energy).[4] In a conventional *p-n* junction device, the absorber layer is *p*-type and the window layer is a large band gap *n*-type transparent semiconductor (e.g., ZnO). To form an efficient *p-n* junction device, the absorber and the window layers should have good compatibility in their crystal and electronic band structures so that the recombination due to the interface states can be minimized. An efficient electron–hole (e–h) separation at a well matched *p-n* junction would ensure a better conversion efficiency of absorbed solar energy.

The compound semiconductors that have matching band gaps (E_g) with the solar spectrum are the binary II-VI and III-V compounds, which include CdTe (II-VI: $E_g \sim 1.5$ eV),[4,11] CdSe (II-VI: $E_g \sim 1.8$ eV),[4] GaAs (III-V: $E_g \sim 1.42$ eV),[11] and InP (III-V: $E_g \sim 1.35$ eV),[11] and ternary

chalcopyrites with a general formula $CuInX_2$ (X = S, Se, and Te: $E_g \sim 1$ to 1.5 eV).[4] The possibility of solid solution formation among the binaries (e.g., $Cd_xHg_{1-x}Te$)[12] and ternaries (e.g., $CuInS_{2x}Se_{2(1-x)}$)[13] would help to tune the energy gap to cover more regions of the solar spectrum and boost the absorption. To prepare and characterize these materials in the one-dimensional (1-D) nanostructural morphology is challenging because of the complex chemistry that involves defects, phase transition and the stability of various phases in the nanometer regime.

Cationic sublattices of zinc-blende, wurtzite and chalcopyrite-type structures are schematically illustrated in Figure 2 to gain an insight into the possible crystal structures that the 1-D nanostructures of II-VI, III-V and chalcopyrite (I-III-VI_2) compounds would adopt. Highlighted in the zinc-blende-type unit cell in Figure 2(a) is the chair configuration that forms as a result of the tetrahedral coordination. This particular arrangement has minimum

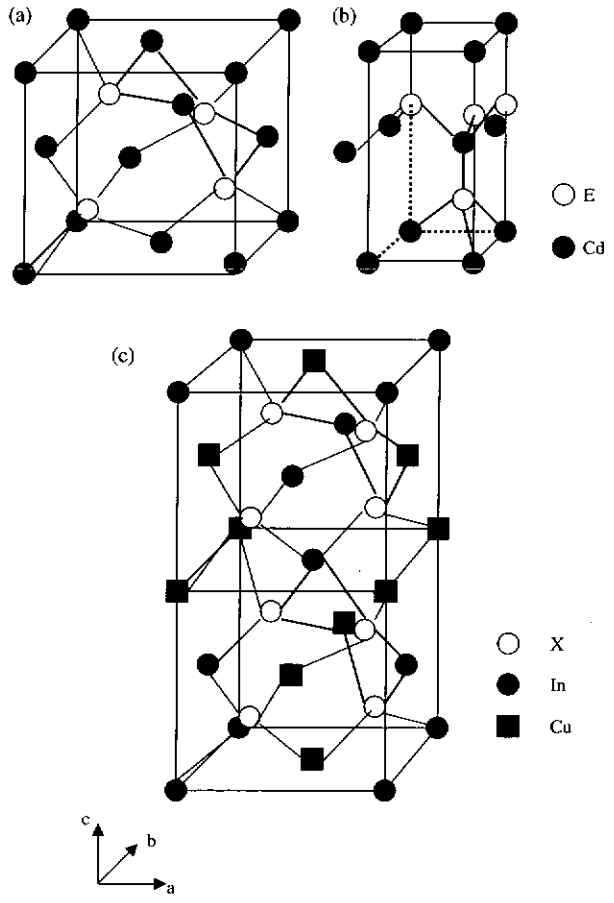

Fig. 2. Cationic sublattices of (a) zinc-blende CdE, (b) wurtzite CdE, E: S, Se, Te, and (c) chalcopyrite-type $CuInX_2$ (X: S, Se, Te) compounds with anions sitting at the tetrahedral sites.[4] The chair configuration is highlighted in zinc-blende CdE and chalcopyrite $CuInX_2$ for comparison. In the wurtzite structure the eclipsed configuration is highlighted. The crystallographic directions a, b, c are indicated for the three types of structures. Reprinted with permission from [4], H. J. Möller, *Semiconductors for Solar Cells*, Artech House Inc., Norwood, MA (**1993**). © (1993), Artech House.

repulsion among the atoms that are covalently bonded as for example in the case of Si or InP.[14] With increasing ionic contribution to the bonding (e.g., CdS or CdSe),[14] the electrostatic attraction between the oppositely charged ions folds the structure so that instead of staggered chair, an eclipsed or boat configuration as highlighted by thick lines in Figure 2(b) is favorable. However, when viewed along the ⟨111⟩ direction, it may be seen that the structures of zinc-blende and wurtzite differ only slightly and hence have very small energy differences (≤20 meV/atom) that leads to polytypism in this type of materials.[15]

Though Yeh et al.[15] in their theoretical calculation have claimed that the zinc-blende-type structure is the preferred crystal structure-type for CdS and CdSe at room temperature, in the nanometer regime, the preference could be altered depending on the processing parameters that include method of preparation, level of supersaturation, temperature, time and so on. In the established procedures of colloidal preparation techniques, nanocrystals can be synthesized as agglomerates without any surface capping or they can be surface-passivated to obtain isolated nanocrystals. The transmission electron microscopic investigation of surface-passivated CdSe nanocrystals[9,14] indicates a hexagonal wurtzite structure. The unsatisfied valences at the surface, and hence the excess surface energy of the nanocrystals has been known to affect the crystal structures and thermodynamic stability of oxides such as γ and α Al_2O_3.[16] In the case of CdS or CdSe, an increased electrostatic stability of the wurtzite would compensate the excess surface energy of nanocrystals, which could be achieved when the structure folds to an eclipsed configuration (Fig. 2(b)). Extending this concept to the possible crystal structures for the 1-D nanostructures of CdS or CdSe, it may be concluded that the 1-D nanostructured CdS or CdSe would prefer the anisotropic wurtzite structure or highly c-axis (001) oriented growth[17,18] to adopt an electrostatically stable structure. But this preference depends on the conditions for the growth of nanostructures. For example, the polytypism of zinc-blende and wurtzite has been identified by Milliron et al.[19] in a recent study that demonstrated the colloidal preparation of heterostructures of branched and linear 1-D nanostructures. They observed a zinc-blende-type region for the primary nucleation of CdTe under high supersaturation. As the level of supersaturation lowered, the anisotropic wurtzite-type CdTe grew from the zinc-blende CdTe junctions. From this result, it may be concluded that at a high supersaturation of the solution, the reduction in surface energy could be achieved in the zinc-blende type structure by spontaneous agglomeration of the growing nuclei. With the reduction in supersaturation of the solution, the excess surface energy of the growing nanocrystals may be compensated by increased electrostatic stability of the crystals in an anisotropic wurtzite structure. Further research on the growth of 1-D chalcogenides for different compositions and under different conditions would help to understand the zinc-blende-wurtzite polytypism in 1-D

chalcogenide semiconductors. Tuning of the electrostatic attraction could be one way to induce an anisotropic growth and realize 1-D nanostructures of chalcogenides, possibly by suitable dopants that generates defects and modifies the career concentration, which may lead to oriented structures with interesting transport properties. Highly oriented 1-D nanostructures of chalcogenides would possibly improve the solar cell performance by acting as efficient channels for electron transport, thereby enhancing the light-to-current conversion efficiency.

Ternary chalcopyrites with a general composition $CuInX_2$ (X = S, Se, Te) exhibit an ordered zinc-blende-type structure. The stacking of the two zinc-blende-type unit cells along the c-axis leads to a tetragonal lattice for the ternary chalcopyrite (Fig. 2(c)). The tetragonality may be evident from their c/a ratio of the unit cell.[4] The intrinsic anisotropy of this family of compounds may be suitable for the 1-D growth of nanorods or wires so that they can be efficient absorber layer for solar cells. But so far there has been only a few reports[20] on 1-D nanostructured chalcopyrites and elucidation of their crystal structures and transport properties. The crystal structure of chalcopyrite consists of a similar cationic sublattice as in the zinc-blende with a distribution of tetrahedrally coordinated Cu and In cations with X. The anion X bonds to two Cu and two In cations. Because of the difference in the ionicity between these two types of bonds, there is intrinsic polarization in the structure, which would lead to tetragonal distortion ($\eta = c/2a < 1$).[21] Zhang et al.[22] in their detailed analysis of defect structure of chalcopyrite $CuInSe_2$ point out that the high defect tolerance of these structures leads to variable Cu/In/Se ratios. Furthermore, the advantages of the $CuInSe_2$ are that the electronic properties can be tuned by introducing native defects without the addition of any extrinsic impurities, the efficient solar energy conversion (~17%) that can be achieved even in the polycrystalline state, and the high resistance to radiation.[23, 24]

Persson and Zunger[24] in a recent theoretical study have modeled the grain boundary in $CuInSe_2$ based on the possible polar surfaces that are neutralized by Cu vacancies to explain the high solar energy conversion efficiency of polycrystalline $CuInSe_2$. The different d-bonding characteristics of the cations with the anion would result in the divergence of the surface energy that is compensated by the low formation energies of Cu vacancies,[22] which are likely to be present on the polar (112) surface of the polycrystalline $CuInSe_2$. Persson and Zunger[24] has put forth the mechanism of formation of Cu vacancies as charge neutralizing defects that stack the polycrystalline $CuInSe_2$ in multiple unit cells in a highly anisotropic fashion. According to their calculation, a barrier exists for the hole to enter from the grain interior to the grain boundary, which is charge-balanced. This barrier would restrict the recombination of electrons and holes at the interfaces and hence result in the high light-to-current conversion efficiency of polycrystalline $CuInSe_2$-based solar cells. The anisotropic stacking model of the chalcopyrite-type $CuInSe_2$ lattice proposed by Persson and Zunger[24] could be of interest to 1-D nanostructured $CuInSe_2$ where an (112)-oriented anisotropic growth would improve the conversion efficiency of the solar cells. The {112} plane is the close-packed plane in $CuInSe_2$ and the growth direction is usually perpendicular to (112) in the ⟨221⟩ direction during the bulk growth.[4] Therefore, the oriented anisotropic (112)-growth of 1-D nanorods/wires of $CuInSe_2$ may be synthetically realized under suitable experimental conditions that generates an ordered defect structure along (112).[24]

3. GROWTH PROCESSES

The growth processes for the 1-D compound semiconductor nanostructures can be classified into three major categories: vapor phase growth, template-assisted synthesis, and solution growth processes. The choice of the method depends on the desired final features of the 1-D nanostructures such as crystallinity, morphology, number density, and amenability to design a device through a 'bottom up' approach. In this section, we will briefly examine the progress in the growth processes of 1-D nanostructures of compound semiconductors (II-VI, III-V, and I-III-VI_2 chalcopyrites) that are the potential candidates in the development of absorber layers in solar cells.

3.1. Vapor Phase Growth

The well-known vapor phase growth procedures are the vapor-liquid-solid (VLS) and vapor-solid (VS) growth processes. The VLS growth proceeds with the assistance of a catalytic film on a substrate (e.g., Au film of a few nanometer thickness on Si) with the nanometer-sized clusters that forms a eutectic alloy either with the substrate (e.g., Au–Si alloy-assisted growth of ZnO nanowires as shown in the atomic force microscopy (AFM) image in Fig. 3)[25] or with the material of interest (e.g., Au-Ga-As alloy-assisted growth of GaAs nanowires).[26] The vaporized material when transported toward the alloy droplet under a suitable career gas, dissolves in the nanometer-sized alloy droplet. Under supersaturation and a suitable temperature gradient, the nanorods/wires grow at the liquid-solid interface, with the catalyst droplets at the tips of the grown 1-D nanostructures. Compared to the progress made in the VLS growth of elemental and ZnO nanostructures, the vapor phase growth of binary II-VI (CdSe, CdTe) and III-V (InP, GaAs) compounds in nanorod/wire morphologies have not been extensively studied. The growth of the 1-D nanostructures of ternary chalcopyrites (e.g., $CuInSe_2$) becomes all the more difficult because of the complex ternary phase chemistry that include variable stoichiometry, thermal expansion and phase transition.[4]

In the recent years, Lieber and coworkers,[26–28] who utilized the laser assisted catalytic VLS growth process to generalize the method for the preparation of II-VI

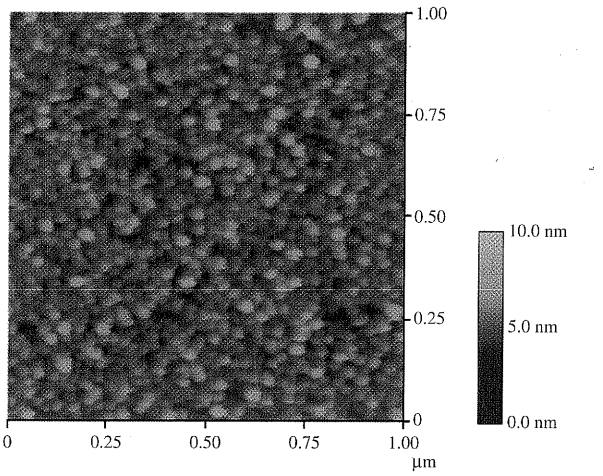

Fig. 3. AFM image of nanometer-sized (~25 nm) Au–Si alloy clusters that assists the VLS growth of 1-D nanostructures in a VLS process. Reprinted with permission from [25], C. Y. Lee et al., *Tamkang J. Sci. Eng.* 6, 127 (**2003**). © (2003), Tamkang University Press, Taiwan, R. O. C.

and III-V compound semiconductors, report excellent control of the diameter and length of the VLS-synthesized nanowires. The candidate materials of interest for the design of absorber layers in solar cells (GaAs, InP, and CdSe) have been synthesized in nanowire form with a minimum radius of ~3–5 nm and lengths up to several micrometers. The single crystallinity in association with a high degree of radial confinement and aspect ratio of these nanowires would make them potential solar cell absorber layers. Under strong confinement, the absorption of solar energy is significantly enhanced, leading to effective separation of electrons and holes. Moreover, the grain boundary effects that degrade the performance of solar cells would be reduced because of the single crystalline feature. Assembling these nanowires in a highly aligned manner would be an immediate task, especially for use in solar cells as absorber layers. To realize this goal, the maturity of the VLS process, which enables the growth of single crystalline and vertically aligned oxide nanorods/wires with controlled number density and tunable aspect ratio (e.g., ZnO),[29,30] and amenability to grow over patterned substrates[31] over a large area, may be exploited to design large-area absorber layers of solar cells. As an example that demonstrates the use of VLS process for the random and vertical growth of 1-D nanostructures, we present the scanning electron micrographs (SEM) of Au and Cu catalyzed ZnO nanowires[29] grown over Si substrate in Figures 4(a) and (b), respectively. The random growth of ZnO nanowires (Fig. 4(a)) could be due to the irregular Au–Si alloy clusters over the substrate, whereas the vertical growth of ZnO with a controlled number density (Fig. 4(b)) may result from the good lattice compatibility of Cu and ZnO.[29] Designing a self-catalytic growth process in which the catalyst and the nanowires are of the same phase would be helpful to synthesize solar absorber layers without metallic impurity. With exotic morphological

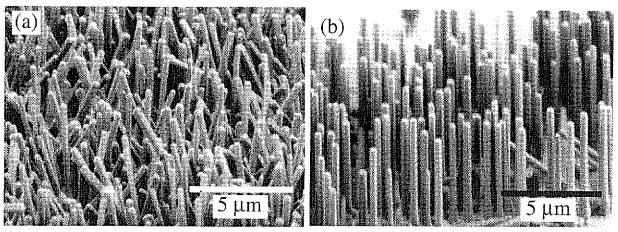

Fig. 4. Demonstration of random and vertical growth of 1-D nanostructures in a VLS process using SEM: (a) Au-catalyzed random growth of ZnO, (b) Cu-catalyzed vertical growth of ZnO with a controlled number density. Reprinted with permission from [29], S. Y. Li et al., *J. Appl. Phys.* 95, 3711 (**2004**). © (2004), American Institute of Physics.

variation such as VLS-grown single crystalline CdSe 'nanosaws,'[32] it would be possible to manipulate the electronic transport, when implemented in a device.

High temperature reported for the VLS growth of GaAs (800–1030 °C), InP (790–830 °C), and CdSe (680–1000 °C)[26] is a prime issue that has to be tackled. In a recent study, Colli et al.[33] report that the Au-assisted VLS growth of single crystalline ZnSe nanowires has been realized at a low temperature of 300 °C using a molecular beam epitaxy (MBE) method. High process selectivity has also been noted on a patterned substrate. Further research could be directed to reduce the VLS growth temperature of compound semiconductor nanowires/rods, possibly through exploitation of low melting alloy clusters or intrinsic strain in a seed layer that provides suitable surface sites for the impinging vapors to nucleate at a low temperature in a low-cost process. An innovative development in the vapor phase growth of semiconductor nanowires is the successful sheathing of VLS grown InP nanowires by layer-by-layer growth of carbon nanotube in a vapor-solid growth process.[34] Carbon with its better stability to different environments would protect the core nanorod/wire-based semiconductor from degradation. A schematic diagram in Figure 5 summarizes the features of VLS or VS-grown morphologies of semiconductor nanostructures over a thin catalytic film or seed layer over a substrate. The morphology III represents VS grown samples in which a random growth and nonuniform shapes are dominant. Nanopyramids, nanosaws, dendrites, or tetrapods can form depending on the processing parameters during the growth. The growth of all other morphological forms may be directed by the catalyst or the seed layer.

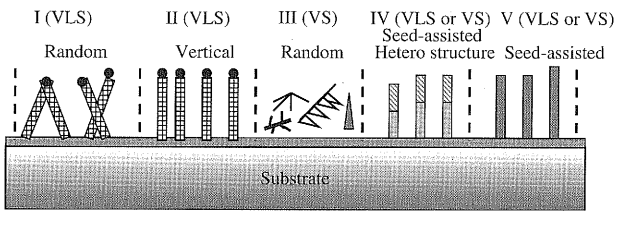

Fig. 5. A summary of morphological variants of compound semiconductors that can be derived from vapor phase growth processes. The thin film on the substrate surface can be a metal catalyst or seed layer that guide the growth front.

3.2. Template-Assisted Synthesis

A highly ordered large-scale array of nanorods/wires on a substrate, with clearly defined number density, morphology, and oriented crystallinity, is the most preferred 1-D nanostructure for direct implementation and testing in devices. To accomplish such a structure, the focus should be on the template-based synthesis of 1-D nanorods/wires. The intrinsic disadvantages such as incomplete filling of the pores, poor wetting of the pore walls, low adhesion to the substrate, and polycrystallinity of the finished product have to be addressed to derive device-quality 1-D nanostructure from a template-based approach. For 1-D nanostructured semiconducting oxides, the template-assisted processing is a well established procedure in which the simplest process is the sol–gel processing inside porous anodic alumina membranes (AAM).[35] In addition to the sol–gel, other techniques such as electrodeposition of 1-D nanorods/wires has been explored for the synthesis of a wide variety of compound semiconductors and composites.[36a, b] The electrodeposition is a viable method for the template synthesis of 1-D nanostructures of chalcogenides, CdX (X = S, Se, Te).[7, 37–39]

Illustrated schematically in Figure 6 is a hybrid structure of polymer and an ordered two-dimensional array of 1-D nanostructure that is obtained after the removal of the template. The polymer phase can be spin-coated or drop-casted over the ordered array to derive a polymer/nanorod hybrid structure. In a typical design of a hybrid solar cell, such an ordered array of 1-D nanostructure is desirable so that the donor phase and the semiconducting nanorod array are in good contact to facilitate an efficient charge transfer.[7] However, a well ordered arrangement of 1-D nanowires/rods of chalcogenides on a large scale is difficult to obtain, possibly because of high surface reactivity or poor mechanical strength that may be overcome when prepared as composites.[40] The present efforts are directed to finding novel template routes. One such method is the sacrificial template route in which microrod arrays of CdOHCl is ion-exchanged with thioacetamide and Na_2SeSO_3 solution to derive 1-D micro or nanostructures of CdS and CdSe, respectively, with a comparable morphology of the sacrificial template.[41] But further research on self-template routes may be required to obtain device quality features of 1-D nanostructures. In a similar procedure that involved multiple ion exchanges, Dloczik et al.[42] started with an ordered vertical columns of ZnO that was electrodeposited over SnO_2:F glass to prepare the chalcopyrite $CuInS_2$. Subsequently, these micro/nanocolumns of ZnO have been ion-exchanged to ZnS to Cu_xS where Cu exhibited a mixed valence state between 1 and 2. The ion-exchanged ZnS-Cu_xS upon treating with In^{3+} led to the formation of coarse $CuInS_2$. The difficulty in retaining the 1-D morphology to the final chalcopyrite phase has been attributed to the 'oxophilic' nature of In^{3+}. Perhaps a simpler route to preparing 1-D nanostructure of chalcopyrites in templates would be to use an electrospray technique[43] (electric-field assisted deposition of a precursor sol in AAM) or dipping in a precursor sol that would fill the pores of AAM with stoichiometric amounts of cations, Cu^{+1} and In^{+3}, which can be later sulphurized or selenized at a suitable temperature to derive a 1-D chalcopyrite nanorods/wires of $CuInS_2$ or $CuInSe_2$. Because of the good solar energy conversion efficiency (~17%)[23, 24] of the polycrystalline forms of chalcopyrite $CuInSe_2$, lack of oriented growth of template-based samples may be compromised for their use as absorber layers in solar cells. An ordered 1-D array of template-derived polycrystalline $CuInSe_2$ would be an attractive candidate for solar cells.

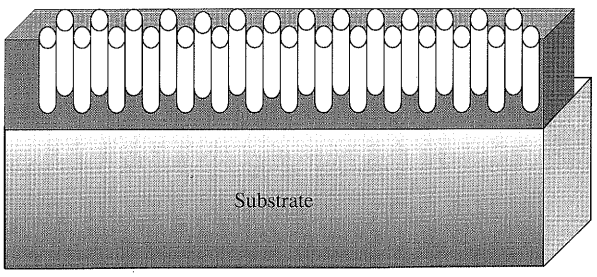

Fig. 6. A hybrid structure of polymer/semiconductor nanorod designed by spin-coating or drop-casting the polymer phase on the substrate so that the gaps of the template-ordered nanorods/wires array are filled uniformly.

3.3. Solution Growth Processes

Solution growth of oriented array of semiconductor nanostructures on flexible substrates at a low cost is attractive in many of the leading technological applications such as field emission devices and ultra-violet (UV) lasers.[44] Currently, there is great interest to explore the solution or colloidal approach for the growth of semiconductor nanostructured absorber layers on flexible substrates to design low-cost solar cells. If the solution-grown nanorods/wires are easily dispersed in a suitable solvent and blended with a donor or polymer phase, then the mixture can be coated on a flexible surface to absorb solar light. The absorbed light is then converted to consumable electric current through a charge transfer process at the polymer/nanorod interface. This technique, which was used by Alivisatos and coworkers to prepare a hybrid polymer/nanorod solar cell of poly(3-hexyl thiophene) (P3HT) and CdSe nanorods,[6] may be further developed to prepare flexible solar cells. The tunable aspect ratio of solution-grown nanorods/wires would help to optimize the solar energy absorption and improve charge carrier mobility. In this backdrop, it is useful to examine the progress in solution growth processes that can yield size- and shape-selected nanorods/wires.

Solution growth processes for 1-D nanostructures is a complex process that depend on numerous factors such as

temperature, concentration, interfacial free energy, solvation enthalpy, and entropy. All these factors would contribute to the two important free energy terms: the surface free energy, which is the energy required to create a new surface and it is positive, and the volume free energy that compensates the positive surface free energy by formation of bonds.[45] Under a high supersaturation in solution, 1-D growth of clusters is not favorable because of the spontaneous and random nucleation. At a moderate saturation, the primary nuclei formed would act as seeds for further kinetically controlled aggregation of clusters to linear chains, possibly aided by the anisotropy of the growing surface. Temperature also has a crucial role in the cluster aggregation process, which can be modeled according to the fractal growth that results from the temperature-dependent processes in colloids: reaction limited aggregation (RLA) and diffusion limited aggregation (DLA).[46] Moreover, in contrast to the fractally smooth spherical surface with a surface fractal dimension of 2,[45] the linearly aggregated 1-D chains of clusters may be considered as a fractally rough object with a high surface energy. This instability has to be compensated by factors such as the anisotropy of the growing crystals, surface passivation, solution growth parameters, or supercritical conditions of solvothermal technique.[47]

The size-selected solution growth of semiconducting II-VI and III-V nanoparticles have been well known with reports of arrested precipitation, synthesis in structured medium such as zeolites, and using molecular precursors and surface capping agents, leading to nanoparticles with a narrow size distribution.[48] In a typical synthesis of rod-shaped CdE (E = S, Se, or Te) nanocrystals, the chalcogenide precursor is injected into a solution containing Cd-precursor in a hot coordinating solvent (~300 °C).[19,49] The formation of CdE nanorods depends on the concentration of the chalcogenide precursor and its injection rate into the cationic solvent. The driving force for the growth of rod-shaped CdE crystals has been attributed to the high chemical potential of the chalcogen in solution during its injection that favors an oriented attachment of the monomers along the c-axis of the growing crystal.[49,50] Using this method, different types of nanorod heterostructures such as CdS/CdTe/CdS and CdTe/CdSe/CdTe have been realized by a suitable sequence of precursor injection.[49] The alkyl phosphonic acids that are used as the surface passivating agent affect the rate of growth of various crystallographic surfaces through its preference for better coordinating capability to Cd^{2+} terminated surfaces than to the Se^{2-} terminated surfaces so that the resultant difference in surface energy promotes anisotropic growth[51] (Fig. 7(a)).

By switching between thermodynamic and kinetic parameters, it is possible to tune the type of growth between the polytypes of the desired phase. An example of such a type of growth is the zinc-blende-wurtzite polytypism in CdE that has been discussed in detail by

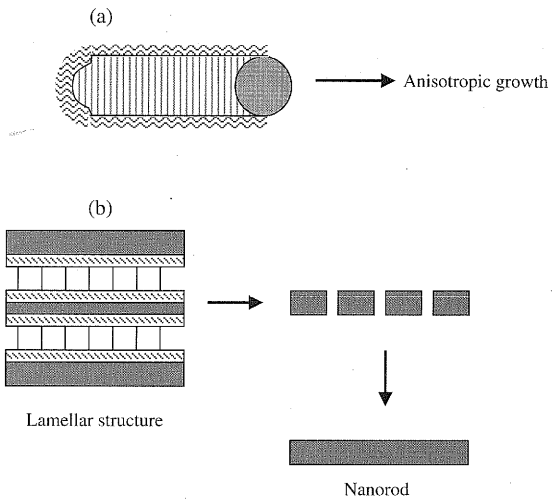

Fig. 7. (a) A schematic illustration of incomplete passivation of nanorod (indicated by vertical lines) surface, leading to anisotropic growth along the nonpassivated high-energy surface. (b) Schematic sequence for ethylene diamine(*en*)-assisted solvothermal synthesis of nanorods through a lamellar intermediate that has CdE layers (dark) separated by *en* ligands (lines). The *en* decomposes on heating to give cracked nanorods, which upon further crystallization yield nanorods.[53] Reprinted with permission from [53], Z. X. Deng et al., *Inorg. Chem.* 42, 2331 (**2003**). © (2003), American Chemical Society.

Manna et al.[51] for CdSe, and has been demonstrated recently for the solution growth of branched heterostructures of CdTe and CdSe.[19] Some of the recent noteworthy efforts in the solution synthesis of semiconductor nanorods are directed to using low toxic starting materials (e.g., $Cd(O_2CCH_3)_2$) instead of the toxic $Cd(CH_3)_2$ for CdE,[52] developing novel solvothermal technique involving coordinating solvents such as ethylene diamine[53] or cetyltrimethyl amine[54] which readily favor the growth of nanorods of CdE or III-V, respectively, through a layered intermediate (Fig. 7(b)), solution-liquid-solid (SLS) growth process for the synthesis of III-V compounds,[55] and tailoring of polymer/nanorod interface for better solar energy conversion efficiency.[56,57] The colloidal preparative route[58] that leads to InP quantum rods with no metallic impurity and excellent size-selectivity would make it possibly a better route than SLS. The reproducible growth of shape- and size-selected nanoparticles or nanorods of ternary chalcopyrites has remained as a challenge because of the difference in coordination chemistry of the two cations. A few reports on 1-D nanowhiskers of $CuInSe_2$[20] and nanoparticles of $CuInS_2$,[59,60] $CuInSe_2$,[61] and $CuInTe_2$[61] focus on the crystallinity, morphology, and size-selectivity of nanostructures in this family of semiconductors.

4. NANOROD-BASED SOLAR CELLS

There has been only a few reports[6–8,10] so far on the preparation and characterization of nanorods as absorber layers in solar cells. In a typical solar cell in which the absorber layers are 1-D nanostructured as schematically illustrated

in Figure 1(a) for the *p-n* junction, the 1-D nanostructures can be self-assembled or drop-casted or spin-coated over the substrates to form a layer of 1-D nanostructure over which an *n*-type layer can be deposited. Alternatively, the *p-n* junction can be grown as a 1-D nanoheterostructure for lattice-matched and oriented anisotropic structures as demonstrated by Bae et al.[62] In their study, they reported the growth of 1-D ZnO over pre-grown semiconducting nanorods such as carbon nanotubes, GaN and GaP nanowires, and SiC core-C-shell coaxial nanocables through a self-catalyzed VLS process. These types of heterostructures would be of particular interest to solar cells, as the *p-n* heterojunction is a single 1-D nanostructure in which the charge carriers are confined. This confinement would probably lead to effective electron–hole separation at the respective electrodes and hence higher conversion efficiency of solar cells. Sequential growth of *p*-type and *n*-type materials in anodic alumina membranes (AAM)[63] would be another feasible approach to design an ordered array of *n*-type window and *p*-type absorber layers for solar cells. The solution of growth of *p-n* heterostructure is an attractive option because of its low cost and the ability to switch the thermodynamic and kinetic parameters to control the growth.[19, 51] But these heterostructures, whether grown by vapor phase, template, or solution process, have yet to be prepared and tested in a solar cell device structure, possibly because of the inability to derive large-scale arrays with good surface and mechanical stability.

The nanorod-based solar cells that are recently prepared and characterized[6–8, 10] have a hybrid structure in which the electron-accepting nanorods are in contact with an electron-donating polymer phase. In these types of hybrid nanostructures, the polymer or donor (D) phase and the semiconducting nanorods or acceptor (A) phase have large interfacial area along which the effective charge transfer would take place. Such interpenetrating and phase-separated D–A networks have been found to improve the career collection efficiency and energy conversion efficiency of polymer photovoltaic cells with the help of a suitable electrode.[64]

The charge transfer process at the nanorod/polymer interface can be experimentally verified by the photoluminescence (PL) measurements. The quenching of the PL signal is indicative of the exciton dissociation or charge transfer at the nanorod/polymer interface, as there is no longer a radiative decay from the excitons.[7, 65] The charge transfer depends on the electron affinities of the nanorods ($E_{A,n}$) and polymer ($E_{A,p}$), electrostatic binding energy of the exciton in the polymer (U_p), and the electrostatic attraction between the electrons and holes (V_{ct}) in the charge-separated state.[65] The condition for the charge transfer can be written as:

$$E_{A,n} - E_{A,p} > U_p - V_{ct} \tag{1}$$

Suitable modification of the polymer chains or size of the nanorods/crystals would tune the above condition, so that the driving force for the charge transfer at the nanorod/polymer interface may be enhanced.

In a hybrid structure of polymer and an inorganic semiconductor nanorod, the charge transport through the system under an applied bias in the dark or under illumination is determined by the disordered charge transport through the polymer and an ordered band-like conduction through the nanorod.[8] To elucidate the charge transport in such a hybrid polymer/nanorod structure, Huynh et al.[8] considered the photovoltaic (PV) cell as a diode that has a photocurrent source, capacitance, and shunt resistance in parallel and a resistance in series. A schematic diagram of current-voltage (*I-V*) curves in the dark and under illumination of a typical *p-n* junction PV device in Figure 8 indicates the important parameters that are to be considered for the charge transport through a PV cell. The fill factor (*FF*), which determines the power conversion efficiency (η) of the PV cell, can be expressed as:

$$FF = \frac{V_m I_m}{V_{oc} I_{oc}} \tag{2}$$

where V_m and I_m are the maximum possible voltage and current output of the shaded rectangular region in the Figure 8, and V_{oc} and I_{sc} are the open circuit voltage and the short circuit current.[4] The conversion efficiency (η) can then be related to the fill factor by the following expression:

$$\eta = \frac{V_m I_m}{P_i} = \frac{FF V_{oc} I_{sc}}{P_i} \tag{3}$$

where P_i is the power of the incident light. Under illumination, all parameters in the Eqs. (2) and (3) are dependent

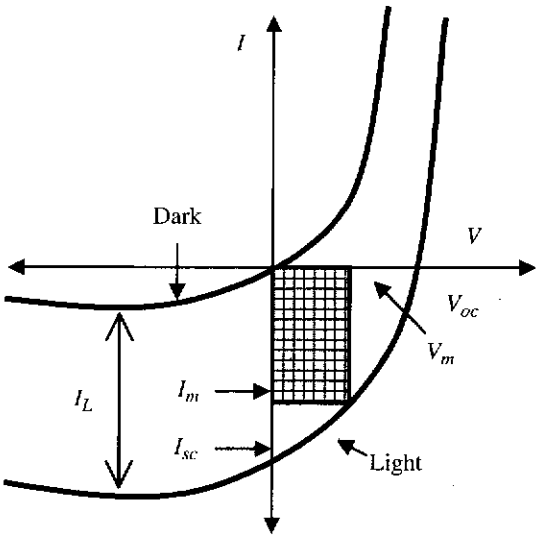

Fig. 8. Parameters that determine the performance of a nanorod-based solar cell illustrated with the help of schematic current-voltage (*I-V*) curves in the dark and under illumination for a typical *p-n* junction device.[4] I_L—current under illumination, I_{sc}—short-circuit current, I_m—maximum current out put, V_{oc}—open circuit voltage, V_m—maximum output voltage. The shaded rectangular region is the fill factor (*FF*). Reprinted with permission from [4], H. J. Möller, *Semiconductors for Solar Cells*, Artech House Inc., Norwood, MA **(1993)**. © (1993), Arytech House

on the wavelength of the incident light.[8] The energy conversion efficiency of a solar cell is therefore directly related to the V_{oc} or I_{sc}, which in turn is determined by the material characteristics such as the lifetime and mobility of the charge careers, and the electron–hole recombination. For instance, in a nanorod/polymer hybrid PV cell that is characterized by a low hole mobility in the polymer phase, under a sufficiently high applied electric field and under illumination, a space charge is generated in the system that opposes the applied field so that the conventional Shockley model for *I-V* characteristics of a diode gets modified through a space-charge approach.[8] The space-charge effect has been found to reduce the external quantum efficiency (EQE) of CdSe/poly-(3-hexyl thiophene) (P3HT) PV device when the applied voltage is in the forward bias. When the device is forward-biased, the space charge effect opposes the applied field, thereby the number of electrons arriving at the external electrode per incident photon (EQE) is reduced. Under the reverse potential, the EQE increases because of the opposite effect. The space-charge effects would also result from the random distribution of the nanorods in the polymer. In such a configuration in which the thickness of the active layer is higher than the length of the nanorods, the 1-D nanostructures do not act as single channels for charge transport. Vertically aligned and longer nanorods would have less space-charge effects and hence better light-to-current conversion efficiency, when implemented as absorber layers in solar cells.

Under high intensity of the incident light, more excitons are generated and they recombine at the polymer/nanorod interface, unless they are efficiently transported to the respective electrodes. This recombination of excitons can be regulated by suitable modification of the polymer chains[8] or the nanorod morphology[10] or the polymer/nanorod interface using suitable surfactants in a colloidal approach.[56, 57] The best performance that has been reported for the nanorod hybrid solar cell is the ~7% monochromatic power conversion efficiency with an EQE of over 54% for the hybrid CdSe/P3HT based solar cells at λ = 515 nm. Under AM 1.5 Global solar radiation the reported power conversion efficiency was 1.7%.[6] The subsequent studies on the tetrapod CdSe/OC_1C_{10}-PPV[10] and the CdTe nanorod/poly(3-octylthiophene) (P3OT)-based[7] solar cells report a comparable conversion efficiency of 1.8% for CdSe/OC_1C_{10}-PPV and a less conversion efficiency value of 1.06% for CdTe nanorod/poly(3-octylthiophene) (P3OT) CdTe nanorod/poly(3-octylthiophene) (P3OT) under AM 1.5 Global solar conditions, respectively. The present review indicates that further intense research, which focuses attention individually on the polymer and nanorod phase, and the successful integration of these components in a final device structure, is required to derive a standard performance from the nanorod-based hybrid solar cells. Moreover, assembling the absorber layer nanorods with a range of diameters would be an attractive design to tune the solar energy absorption as proposed by Mehta and

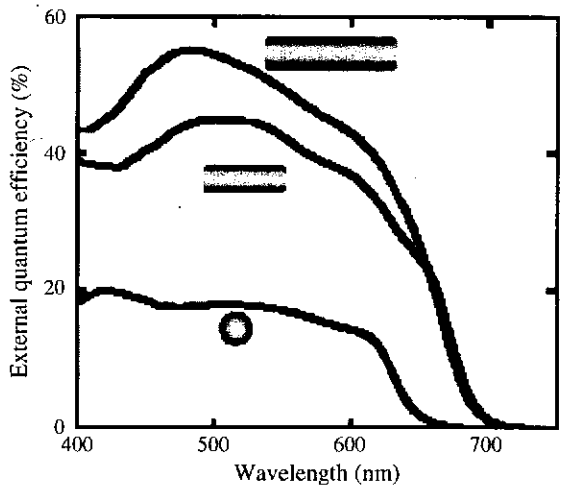

Fig. 9. Tunable external quantum efficiency (EQE) of 7 nm diameter CdSe nanorods with lengths 7 nm, 30 nm, and 60 nm.[6] Reprinted with permission from [6], W. U. Huynh et al., *Science* 295, 2425 (**2002**). © (2002), Science, AAAS.

Kruis[66] in a conceptual device proposal. Nanorods with fixed diameters, but having different lengths affect the EQE under illumination. A 60 nm long CdSe nanorod with a diameter of 7 nm exhibits a higher EQE than 30 nm long CdSe nanorods and the spherical CdSe in a hybrid structure with a polymer (Fig. 9).[6] The major factors that affect the EQE are the intensity of the incident light, light absorption, charge carrier collection efficiency at the electrodes and charge transfer process at the nanorod/polymer interface. Assuming that all these parameters were same for their devices with CdSe nanorods of different aspect ratios, Huynh et al.[6] have explained that the higher EQE (~3 times) of 60 nm long CdSe nanorods could have been due to the enhanced one-dimensional charge transport. In the following section, the performance of these nanorod-based solar cells is compared with dye-sensitized and organic solar cells.

5. COMPARISON WITH DYE-SENSITIZED AND ORGANIC/POLYMER SOLAR CELLS

The compound semiconductors that have been discussed so far have the advantages of high spectral match with the solar spectrum, but there are certain critical issues such as the high toxicity of Cd or As, low abundance of In for chalcopyrite-type cells, complex ternary phase chemistry of chalcopyrites, and the inability to grow chalcogenides and chalcopyrites over a large area with good surface and mechanical stability. These issues have generated great motivation to find alternative designs for solar cells. The two important categories are the dye-sensitized and organic structure-based photovoltaic devices. An exhaustive review of these alternative designs is not the objective of this article. But a comparison of these solar cell structures to the nano 1-D inorganic absorber

layer-based solar cells would help to assess the merits and demerits of these types of structures, and possible strategies to improve the cell performance.

5.1. Dye-Sensitized Solar Cells

Some examples of dye-sensitized and organic solar cells are presented in Table I along with the nanorod-based hybrid solar cells. The configurations and the important characteristics of these cells are listed in the second and third column, respectively. The power conversion efficiency, η, of the dye-sensitized solar cells are relatively higher than the nanorod-based hybrid cell and organic or polymer cell. A maximum η of about 10% has been achieved in a TiO_2-based dye-sensitized solar cell.[67] The high η of the dye-sensitized structure can be

Table I. Characteristics of nanorod-based, dye-sensitized, and organic/polymer solar cells.

Solar cell type	Configuration	Characteristics	Ref.
Hybrid nanorod/ polymer	Glass/ITO/PEDOT-PSS/ (CdSe Nanorod-P3HT)/Al	AM 1.5 Global solar condition: $\eta \sim 1.7\%$, $V_{oc} \sim 0.7$ V, $J_{sc} \sim 5.7$ mA/cm^2, $FF \sim 0.4$	[6]
Hybrid nanorod/ polymer	Ti/(CdTe Nanorod-P3OT)/Au	AM 1.5 Global solar condition: $\eta \sim 1.06\%$, $V_{oc} \sim 0.714$ V, $J_{sc} \sim 3.12$ mA/cm^2, $FF \sim 0.48$	[7]
Hybrid tetrapod/ polymer	Glass/ITO/PEDOT-PSS/ (CdSe Tetrapod-OC_1C_{10}-PPV)/Al	AM 1.5 Global solar condition: $\eta \sim 1.8\%$, $V_{oc} \sim 0.65$ V, $J_{sc} \sim 7.30$ mA/cm^2, $FF \sim 0.65$	[10]
Dye-sensitized photoelectrochemical cell	Conducting glass/colloidal TiO_2/Dye	AM 1.5 Global solar condition: $\eta \sim 7$ to 8%, $FF \sim 0.685$ to 0.76 Diffused day light: $\eta \sim 12\%$, $FF \sim 0.7$	[3]
Dye-sensitized photoelectrochemical cell	Conducting glass (SnO_2:F)/Nanocrystalline TiO_2/Dye/Electrolyte/Counter electrode	500 W Xe Lamp: LiI as Electrolyte: $\eta \sim 1.23\%$, $V_{oc} \sim 0.52$ V, $J_{sc} \sim 3.42$ mA/cm^2, $FF \sim 0.58$	[68]
Dye-sensitized photoelectrochemical cell	Glass/ITO/TiO_2/TiO_2 Nanowires/Dye	AM 1.5 Global solar condition: $\eta \sim 9.3\%$, $V_{oc} \sim 0.72$ V, $J_{sc} \sim 19.2$ mA/cm^2, $FF \sim 0.675$	[70]
Dye-sensitized hybrid structure	Glass/ITO/ P3OT-SWCNT + Dye-composites/Al	AM 1.5 Global solar condition: $\eta \sim 0.036\%$, $V_{oc} \sim 0.6$ V, $J_{sc} \sim 0.18$ mA/cm^2, $FF \sim 0.35$	[71]
Hybrid polymer/ Nanocrystal photoelectrochemical cell	Conducting glass (SnO_2:F)/Carboxylated polythiophene-Nanocrystalline TiO_2/ Electrolyte/ Counter electrode	AM 1.5 Global solar condition: $\eta \sim 1.4\%$, $V_{oc} \sim$ —, $J_{sc} \sim 8$ mA/cm^2, $FF \sim$ —	[72]
Dye-sensitized photoelectrochemical cell	Conducting glass (SnO_2:F)/ZnO Nanowires/ Dye/Electrolyte/Counter electrode	100 mW/cm^2 broadband illumination by tungsten halogen-lamp: $\eta \sim 0.5\%$, $V_{oc} \sim 0.74$ V, $J_{sc} \sim 1.62$ mA/cm^2, $FF \sim 0.38$	[73]
Donor–Acceptor blend solar cell	Glass/ITO/CuPC-PTCBI/Top electrode	AM 1.5 Global solar condition: $\eta \sim 2.7\%$, $V_{oc} \sim 0.50$ V, $FF > 0.5$	[93]
Donor–Acceptor blend solar cell	Glass/ITO/PEDOT/MDMO-PPV:MethanoC60/LiF/Al	AM 1.5 Global solar condition: $\eta \sim 2.5\%$, $V_{oc} \sim 0.82$ V, $J_{sc} \sim 5.25$ mA/cm^2, $FF \sim 0.61$	[96]
Donor–Acceptor blend solar cells	Glass/ITO/MEH-PPV-C60/Al (high C60 content denoted by structure P2)	Monochromatic light: 500 W Xenon lamp: $\eta \sim 0.01\%$, $V_{oc} \sim 0.6$ V, $J_{sc} \sim 0.06$ mA/cm^2, $FF \sim 0.27$	[98]
Three-layer organic cell (Donor–Acceptor)	Glass/Al/PV/Porphyrine/MC/Au	445 nm monochromatic light: $\eta \sim 3.51\%$, $V_{oc} \sim 0.39$ V, $\phi \sim 0.492$, $FF \sim 0.51$	[100]
Heterojunction organic/ organometallic solar-cells (Donor–Acceptor)	Glass/ITO or ZnO/PEDOT:PSS/ Zn-Pc/DAAQ/Al	AM 1.5 Global solar condition: $\eta \sim 0.007\%$, $V_{oc} \sim 0.88$ V, $J_{sc} \sim 1.4 \times 10^{-2}$ mA/cm^2, $FF \sim 0.57$	[101]
Schottky *p-n* junction solar cells	Glass/ITO/8T/DPP/Al	Monochromatic light, tungsten halogen lamp: Random orientation of 8T molecules $\eta \sim 6.5$ to $7 \times 10^{-4}\%$, $V_{oc} \sim 0.50$ to 0.57, $FF \sim 0.17$ to 0.19	[103]
Bulk heterojunction Donor–Acceptor solar cell	Glass/ITO/PEDOT:PSS/P-*m*-MTDATA/ZnPc:C60/*n*-MPP/LiF/Al	AM 1.5 Global solar condition: $\eta \sim 3.37\%$, $V_{oc} \sim 0.45$ V, $J_{sc} \sim 1.5$ mA/cm^2, $FF \sim 0.5$ (1/10 sun, 10 mW/cm^2)	[104]
Hetero junction solar cell (Donor–Acceptor)	Glass/ITO/PEDOT/CY-5/C-60/Al	Monochromatic light, tungsten halogen lamp: $\eta \sim$ —, $V_{oc} \sim 0.41$ to 0.43 V, $J_{sc} \sim 1.0$ to 1.4×10^{-4} A/cm^2	[105]
Donor–Acceptor blend solar cells	Glass/ITO/Perylene-MEH-PPV/Al	Monochromatic light, 0.1 mW/cm^2, Tungsten lamp: $\eta \sim$ —, $V_{oc} \sim 0.37$ V, $\phi \sim 0.71$, $FF \sim 0.44$	[106]

Expansion of symbols and abbreviations:
η: Power conversion efficiency, V_{oc}: Open circuit voltage, J_{sc}: Short circuit current density, *FF*: Fill factor, AM: Air Mass, P3HT: Poly-3(hexylthiophene), OC_1C_{10}-PPV: Poly(2-methoxy-5-(3′,7′-dimethyl-octyloxy)-*p*-phenylenevinylene), P3OT: Poly-3(Octylthiophene), SWCNT: Single-walled carbon nanotubes, ITO: Indium tin oxide, PV: Perylene-3, 4, 9, 10-tetracarboxyl-bis-benzimidazole, MC: (3-Carboxymethyl-5-[(3-ethyl-2(3H)-benzothiazolylidine)ethylidene]-2-thioxo-4-thiazolidinone), PEDOT: Poly(3,4-ethylene dioxythiophene), PSS: Poly-(styrene sulfonate), Zn-Pc: Zinc phthalocyanine, DAAQ: Diaminoanthraquinone, MEH-PPV: poly(2-methoxy-5-(2′-ethyl-hexyloxy)-*p*-phenylene vinylene), Cy5: 1,1′-diethyl-3,3,3′,3′-tetramethylcarbocyanine perchlorate, 8T: Octylthiophene, DPP: N,N′-diphenyl 3,4,9,10-perylenetetracarboxylic-diimide, MTDATA: 4,4′,4″-tris(3-methylphenylphenylamino)triphenylamine, MPP: dimethyl-perylene-tetracarboxylic-diimide, MDMO-PPV: Poly[2-methyl, 5-(3′, 7″dimethyl octyloxy]-*p*-phenylene vinylene), C60: Fullerene, CuPc: Copper phthalocyanine, PTCBI: 3,4,9,10-perylenetetracarboxylic bis-benzimidazole.

explained based on the kinetics of electron transfer process at the interface between the dye (e.g., N3:tri(cyanato)-2,2′,2″-terpyridyl-4,4′,4″-tricarboxylate ruthenium(II)), the semiconductor (e.g., mesoporous TiO_2), and the electrolyte. A schematic energy level diagram in Figure 10 traces the possible time-dependent electron transfer processes at the semiconductor (TiO_2)-dye (N3)-electrolyte interface.[67] The electron transfer at the dye-semiconductor interface is in the femto second (fs) regime that is much faster than all other possible transfers and hence may be one of the reasons for the high η of the dye-sensitized solar cells. But subsequent electron transfer processes such as the conduction through the semiconductor, collection efficiency of the electrode, and restoration of the original electronic state of the dye are equally important as the sustained light-to-current conversion depends on these processes. For instance, the relatively slow process at the electrolyte/dye interface might cause space charge effect and degradation in performance over a period of time. Furthermore, the nature of the electrolyte and the solvent in the photoelectrochemical cell affect the photovoltaic properties by causing a shift in the conduction band of the TiO_2 electrode.[68,69]

The high conversion efficiency of the dye-sensitized cell would also result from the increased electronic conductivity of the mesoporous semiconducting oxide layer. The conduction mechanism in this semiconducting mesoporous oxide layer may be attributed to the random walk of electrons through shallow or deep potential wells.[67] With increasing intensity of the incident light, electrons fill the deep potential wells under steady-state and the transport is enhanced due to the hopping of electrons through the shallow traps in the oxide layer. Elimination of electron traps

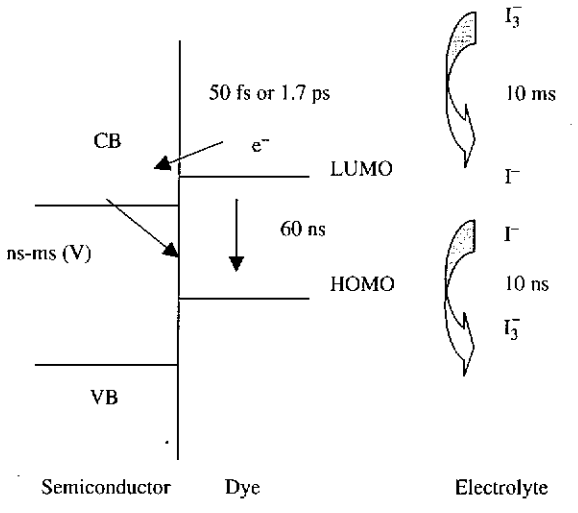

Fig. 10. Schematic energy level diagram illustrating the kinetics of electron transfer processes at the TiO_2/N_3/Electrolyte interface.[67] The time required for the various steps of electron transfer is indicated as fs, ps, ns, or ms. Reprinted with permission from [67], A. Hagfeldt and M. Grätzel, *Acc. Chem. Res.* 33, 269 (**2000**). © (2000), American Chemical Society.

at the grain boundaries could be achieved when TiO_2 is prepared as single crystal nanowires.[70] The single crystal 1-D nanostructure of TiO_2 would act as efficient channels for electronic conduction, which is similar to the enhanced carrier transport through the 1-D semiconductor absorber layers as discussed earlier. Moreover, the high surface area of the TiO_2 nanowires enables adsorption of more dye molecules on the TiO_2 nanowires than on the TiO_2 nanoparticles, thereby improving the photovoltaic characteristics.[70]

In a composite structure of single-walled carbon nanotubes (SWCNT), P3OT polymer, and a dye at the interface between the polymer and the SWCNT in a solar cell configuration, the short circuit current density of the device is enhanced in the presence of the dye.[71] Though this composite structure has a low conversion efficiency (~0.036%), the basic principle may be extended to nanorod-based hybrid solar cells. High surface area of the absorber layer nanorods may be exploited to sensitize its surface with a dye to enhance the charge transfer process. However, such a structure is complex because of the obvious increase in the number of interfaces, time-regimes for the charge transfer processes, and the stability of the dye. The current density-voltage curves for the cells ITO/P3OT-SWCNT/Al (Fig. 11(a)) and ITO/P3OT-SWCNT + PM (Dye: *N*-(1-pyrenyl)maleimide)/Al (Fig. 11(b)) indicate that, under illumination, the open circuit voltage and the short circuit current density of the device with dye are higher than that without the dye. The improved photovoltaic performance in the presence of dye at the interface between the nanotube and the polymer may be due to the efficient charge transfer process in which an electron is transferred from the photoexcited dye to the conduction band of the nanotube followed by a hole transfer to the highest occupied molecular orbital (HOMO) of the P3OT polymer. A recent study demonstrates that by suitable modification of the functional groups of the polymer (e.g., carboxylated polythiophene), the charge transfer process can be tuned at the polymer /TiO_2 interface in the absence of dye sensitizer.[72]

The advantage of dye-sensitized solar cells is that the nontoxic materials such as TiO_2 and ZnO could be grown as 1-D nanostructures, which may be later sensitized and assembled in a photovoltaic device configuration. For example, very recently, random and vertical growth of 1-D nanostructured ZnO has been exploited to design a dye-sensitized structure with an energy conversion efficiency of ~0.5%.[73] The successful synthesis of high surface area semiconducting oxides (TiO_2,[74–80] ZnO,[24,29,30,44,81–83] SnO_2,[84,85] In_2O_3,[86] α-Fe_2O_3,[87] Co_3O_4,[88] and CuO[89]) in various 1-D nanostructured morphologies using different methods on a large scale and ordered array would enable further improvement in the solar cell conversion efficiency of dye-sensitized structure. However, there may be some limitations for the design of large area solar cells in the dye-sensitized structure, when the cells use a liquid electrolyte. Furthermore, as compared to the nanorod-based

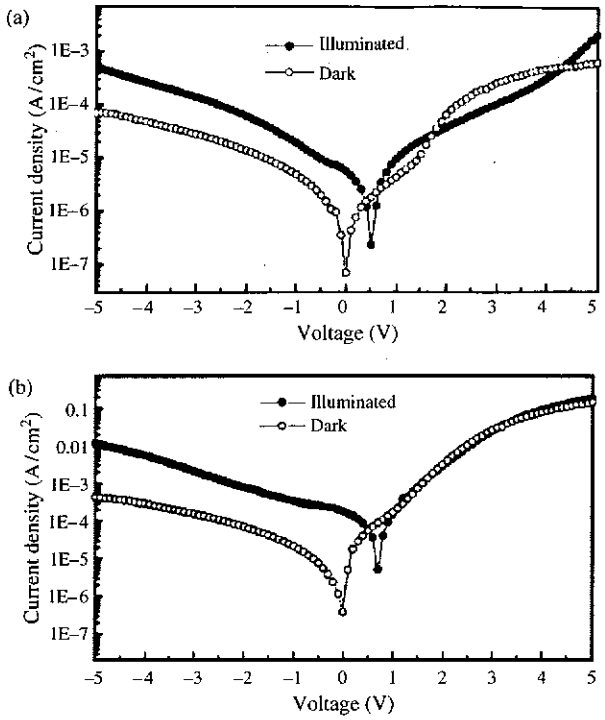

Fig. 11. Current density-voltage characteristics for the solar cells with configurations (a) ITO/P3OT-SWCNT/Al, and (b) ITO/P3OT-SWCNT+ PM (Dye: *N*-(1-pyrenyl)maleimide)/Al under dark and under illumination (AM 1.5 Global solar radiation). Reprinted with permission from [71], S. Bhattacharya et al., *Chem. Mater.* 16, 4819 (**2004**). © (2004), American Chemical Society.

hybrid solar cells, the dye-sensitized structure is limited by the stability and adhesion of the dye on the nanostructured oxide layer, various electron transfer processes at the semiconductor/dye/electrolyte interfaces, and the stability of the electrolyte. The cell may require longer testing cycles to confirm its conversion efficiency, which is determined by the complex electron transfer kinetics as illustrated in Figure 10. In contrast, a hybrid structure of absorber layer solar cells may be readily prepared by processes that involve less number of steps: self-assembly of the 1-D absorber layer nanorods, and subsequent filling of the inter-rod spacing with a suitable polymer using spin or drop-cast techniques. The 1-D absorber layer-based hybrid solar cells are also potential candidates for the design of flexible solar cells.

5.2. Organic/Polymer Solar Cells

Organic or polymeric materials have been at the forefront of photovoltaic research to compete with the costly Si solar cells. The advantages of using an organic solar cell are the relatively inexpensive material costs, low-cost deposition process, ability to coat large area over flexible substrates using techniques such as screen printing, compatibility in various integrated devices, and the ecological benefits[90] as compared to the toxic Cd or As. A typical organic solar cell has a planar configuration in which the organic material is sandwiched between the two electrodes. Upon excitation of an electron from the HOMO to lowest unoccupied molecular orbital (LUMO) under illumination, an exciton is generated and the resultant conversion efficiency of the cell depends on the subsequent extraction of electrons and holes at the respective electrodes.[91] But conversion efficiencies (<5%) of organic solar cells are still far less than the Si solar cells. While the nanorod absorber layer-based hybrid solar cells have conversion efficiencies of ~1–2%, the reported conversion efficiencies of organic solar cells fall in a broad range with the lower limit touching $\sim 10^{-4}$–10^{-3}% and the upper limit of ~3–3.5% (Table I). The large variation in the reported conversion efficiencies indicates the difficulty in extracting steady and consistent electronic transport from organic semiconductors.

A crystalline inorganic semiconductor has the individual HOMO and LUMO of molecules overlapping to form the conduction band and valence band that extends the entire solid. In such a structure, the dissociation of photogenerated excitons under an asymmetric electric field is more favorable than that of the generated excitons in an organic semiconductor, where the excitons are localized to the HOMO and LUMO that do not extend the entire material. The strongly bound excitons in organic semiconductors recombine and thus the charge separation and resultant electron and hole transport are not intrinsically favorable in an organic semiconductor, thereby lowering the electron and hole mobilities.[91] For single component organic solar cell with an active layer thickness of ~100 nm, the diffusion distance of excitons (~10 nm) is much less than the organic layer thickness so that the electrons and holes recombine before they reach the electrode. Reducing the active layer thickness is a possible way to extract the charge carriers at the electrodes, but then the light absorption is limited. The breakthrough came when Tang reported the first heterojunction organic photovoltaic device in which the EQE of the device improved to ~15% because of the enhanced excitonic dissociation at the donor–acceptor interface.[92] In a donor–acceptor blend, the diffusion distance of the excitons and the interfacial thickness match so that the electrons are transferred to the LUMO of the acceptor molecule. Thus, the charge transfer process is enhanced in such a bulk heterojunction structure.[93]

The advantage of hybrid solar cells with an inorganic absorber layer is the intrinsic crystalline anisotropy favoring the one-dimensional (1-D) growth (e.g., CdSe) and hence the directed carrier transport. The excitons that are confined in these 1-D structures dissociate under an asymmetric electric field at the interface with a conjugated polymer. In the field of polymeric photovoltaic research, the recent efforts focus on improving the charge transfer process by using fullerene (C60) as an acceptor in a donor–acceptor blend structure.[94] The high electron affinity, transparency and electronic conductivity (10^{-4} S/cm)

of C60 has made this allotrope of carbon as a favorite choice for the acceptor phase in a donor–acceptor blend structure.[91,95]

A highly efficient polymer-C60 blend solar cell was reported by Yu et al.[64] in 1995. In their study, the cells recorded a conversion efficiency (η) of about 2.9% in a blend of MEH-PPV (poly(2-methoxy-5-(2′-ethyl-hexyl-oxy)-*p*-phenylene vinylene)) and methano C60. The best performance was recorded for the device with a weight ratio of MEH-PPV to C60 as 1:4 and 1,2-dichlorobenzene as the solvent in a bulk interpenetrating donor–acceptor layer of thickness in the range of ~100 to 200 nm. These bulk heterojunctions would have large number of interfaces, where within every few nanometers, there could be a donor–acceptor interface at which the charge transfer process could take place. But the major hurdle in obtaining a sustainable light-to-current conversion efficiency has been the phase separation of the bicontinuous networks to macroclusters, which would lead to degradation of polymer/C60 devices. Shaheen et al.[96] in their recent study claims that by suitable functionalization of the C60 moeity, phase segregation could be prevented and hence led to 2.5% efficiency for their plastic solar cells. Chemically attaching a donor polymer to C60[97] could be one method so that the donor–acceptor blends are formed by chemical bonds rather than the physical binding as in a hybrid structure.

The conjugated polymer oligophenylenevinylene (OPV) and C60 blend in a solar cell device of configuration ITO/OPV : C60/Al exhibits the current-voltage characteristics as shown in Figure 12. Nierengarten[97] reported that this device has a short circuit current density of 10 μA/cm^2 and an open circuit voltage of 0.46 V. It has been claimed that despite its below par performance, the characterization of such a device was the first demonstration of chemically linked bicontinuous donor–acceptor layer in a solar cell configuration. Further research is required in this direction to improve the conversion efficiency of C60-based solar cells. One advantage of molecular photovoltaics is the possibility of interface engineering at the critical length scales of exciton diffusion distance where a donor type molecule can chemically attach to an acceptor-type molecule so that the interface stability and charge transfer can be enhanced.[98] Moreover, the functional groups of the acceptor molecules can be modified to enhance the photovoltaic properties.[99]

A solid-state organic solar cell reported by Takahashi et al.[100] had a porphyrin structure as the active layer that was sandwiched in a three layer structure with an acceptor polymer PV (perylene-3, 4, 9, 10-tetracarboxyl-bis-benzimidazole) and a donor polymer MC (3-Carboxymethyl-5-[(3-ethyl-2 (3H)-benzothiazolylidine) ethylidene]-2-thioxo-4-thiazolidinone). Under photoexcitation, the intermolecular electron transfer takes place from the porphyrin to PV. The donor MC molecules donate the electrons to the porphyrin so that the back-electron transfer to the porphyrin from PV is prevented. This all-organic three-layered solid state solar cell had an EQE of ~49%, open circuit voltage of 0.39 V, fill factor of 0.51, and an energy conversion efficiency of ~3.5%. The principle used in this structure

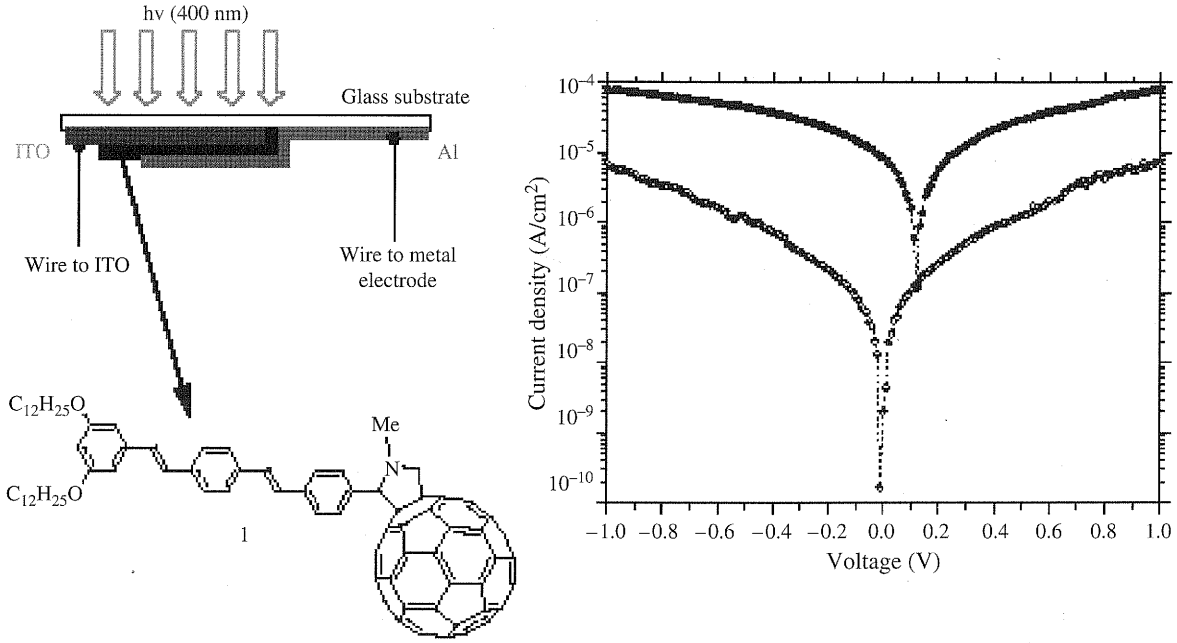

Fig. 12. Current density-voltage characteristics for the solar cell based on chemically attached oligophenylenevinylene (OPV) and C60 in a donor–acceptor bicontinuous network in the dark and under illumination ($\lambda = 400$ nm with an intensity of 12 mW/cm^2). The curve under illumination is shifted from 0 V to the corresponding open circuit potential under illumination. The device configuration and the chemical attachment of the OPV and C60 are shown on the left side of the figure. Reprinted with permission from [97], J. F. Nierengarten, *Sol. Energy Mater. Solar Cells* 83, 187 (**2004**). © (2004), Elsevier.

may be extended to the nanorod-based layered solar cells in which the nanorod-based layer may be sandwiched between the acceptor and donor-type layers. In such a structure, the exciton dissociation may be faster to enhance the conversion efficiency.

With an increase in the number of layers, the interfacial roughness would affect the overall performance of the solar cells. Smooth interfaces have been found to favor higher fill factor in the multilayered organic solar cells.[101] A high fill factor would also lead to higher conversion efficiencies.[102] Apart from the interfacial roughness, intrinsic configuration of organic molecules affects the light absorption and the photocurrent density of octyl thiophene (8T) molecules, when spread over the substrate as a *p*-layer. For example, in comparison with nonplanar configurations of 8T molecules, the planar configuration of 8T on glass/ITO/8T/polymer/Al exhibited high light absorption and improved photocurrent density.[103] This molecular level configuration is in contrast to the nanorod-based solar cells, where nonplanar arrangement of absorber layer nanorods (tetrapods) enhance the light absorption and resultant carrier conduction.[10]

The organic layer may be protected from the Al diffusion and the resultant degradation by coating a thin LiF layer over the organic layer. Similarly, the diffusion of In to the organic layer may be prevented by coating a layer of hole-transporting PEDOT (poly(3,4-ethylene dioxythiophene))-PSS (poly-(styrene sulfonate)) in a device configuration,[104, 105] for example, glass/ITO/PEDOT : PSS/*p*-polymer/Zn-Pc (zinc phthlocyanine) : C60 (fullerene)/*n*-polymer/LiF/Al.[104] A PEDOT-PSS layer over ITO (indium tin oxide) would also help to smooth the uneven electrode surface.[91] The interfacial roughness could be a crucial factor in the absorber layer hybrid nanorod solar cells, where the device configuration is similar to the multilayered organic structure (e.g., glass/ITO/PEDOT-PSS/(CdSe Nanorod-P3HT)/Al).[6] The crystallization of an acceptor phase, perylene, in a blend structure with a donor conjugated polymer yields an improved quantum efficiency of the solar cells, possibly because of the enhanced carrier transport through the ordered perylene phase.[106] The hybrid structure of nanorods and the polymer may be similar to the conjugated polymer-perylene blend with a crystallized nanorod phase that is dispersed in a disordered polymer phase.

6. SUMMARY

One-dimensional (1-D) compound semiconductor nanostructures that belong to the II-VI chalcogenides, III-V, and ternary I-III-VI_2 chalcopyrites with band gaps that match the solar spectrum are promising materials to be used as absorber layers in solar cells. With their high aspect ratio, oriented crystallinity and career confinement, these 1-D nanostructures would act as channels for current conduction when aligned vertically over a substrate. The growth of large scale and ordered array of these 1-D nanostructures would be an immediate challenge for solar cell applications. In a hybrid structure with a polymer or donor phase, the interpenetrating polymer and the nanorod or acceptor phase undergo charge transfer and assist in the power conversion of solar cells. However, the solar cells based on these hybrid polymer/nanorod structures have less power conversion efficiency than the conventional Si solar cells, and therefore, require further research to standardize their performance. Other advancing areas of photovoltaic research such as dye-sensitized and organic/polymer solar cells have been compared with the nanorod-based hybrid solar cells. The comparison shows that the reported conversion efficiencies of dye-sensitized structures are relatively higher than the nanorod-based hybrid structure. The organic/polymer solar cells exhibit a wide range of conversion efficiencies, possibly due to the inability to derive steady and sustainable light-to-current conversion in these types of devices.

Acknowledgments: Authors thank the financial support by the National Science Council of the Republic of China under the Contract No. NSC 93-2216-E009-024.

References and Notes

1. E. J. Moniz and M. A. Kenderdine, *Phys. Today* 55, 40 (**2002**).
2. K. L. Chopra, P. D. Paulson, and V. Dutta, *Prog. Photovolt.: Res. Appl.* 16, 69 (**2004**).
3. B. O. Regan and M. Grätzel, *Nature* 353, 737 (**1991**).
4. H. J. Möller, *Semiconductors for Solar Cells*, Artech House Inc., Norwood, MA (**1993**).
5. J. Hu, T. W. Odom, and C. M. Lieber, *Acc. Chem. Res.* 32, 435 (**1999**).
6. W. U. Huynh, J. J. Dittmer, and A. P. Alivisatos, *Science* 295, 2425 (**2002**).
7. Y. Kang, N. G. Park, and D. Kim, *Appl. Phys. Lett.* 86, 113101 (**2005**).
8. W. U. Huynh, J. J. Dittmer, N. Teclemariam, D. J. Milliron, A. P. Alivisatos, and K. W. J. Barnham, *Phys. Rev. B* 67, 115326 (**2003**).
9. A. P. Alivisatos, *Science* 271, 933 (**1996**).
10. B. Sun, E. Marx, and N. C. Greenham, *Nano Lett.* 3, 961 (**2003**).
11. D. K. Schroder, *Semiconductor Material and Device Characterization*, John Wiley and Sons, New York (**1998**).
12. A. Belaidi, R. Bayón, L. Dloczik, K. Ernst, M. C. L. Steiner, and R. Könenkamp, *Thin Solid Films* 431–432, 488 (**2003**).
13. A. V. Mudryi, I. A. Victorov, V. F. Gremenok, A. I. Patuk, I. A. Shakin, and M. A. Yakushev, *Thin Solid Films* 431–432, 197 (**2003**).
14. A. P. Alivisatos, *J. Phys. Chem.* 100, 13226 (**1996**).
15. C. Y. Yeh, Z. W. Lu, S. Froyen, and A. Zunger, *Phys. Rev. B* 46, 10086 (**1992**).
16. J. M. McHale, A. Auroux, A. J. Perrotta, and A. Navrotsky, *Science* 277, 788 (**1997**).
17. M. Chen, Y. Xie, J. Lu, Y. Xiong, S. Zhang, Y. Qian, and X. Liu, *J. Mater. Chem.* 12, 748 (**2002**).
18. M. Chen and L. Gao, *J. Am. Ceram. Soc.* 88, 1643 (**2005**).
19. D. J. Milliron, S. M. Hughes, Y. Cui, L. Manna, J. B. Li, L. W. Wang, and A. P. Alivisatos, *Nature* 430, 190 (**2004**).
20. B. Li, Y. Xie, J. Huang, and Y. Qian, *Adv. Mater.* 11, 1456 (**1999**).
21. X. Jiang and W. R. L. Lambrecht, *Phys. Rev. B* 69, 035201 (**2004**).

22. S. B. Zhang, S. H. Wei, A. Zunger, and H. K. Yoshida, *Phys. Rev. B* 57, 9642 (**1998**).
23. A. Polity, R. K. Rehberg, T. E. M. Staab, M. J. Puska, J. Klais, H. J. Möller, and B. K. Meyer, *J. Appl. Phys.* 83, 71 (**1998**).
24. C. Persson and A. Zunger, *Phys. Rev. Lett.* 91, 266401 (**2003**).
25. C. Y. Lee, T. Y. Tseng, S. Y. Li, and P. Lin, *Tamkang J. Sci. Eng.* 6, 127 (**2003**).
26. X. Duan and C. M. Lieber, *Adv. Mater.* 12, 298 (**2000**).
27. X. Duan, Y. Huang, Y. Cui, J. Wang, and C. M. Lieber, *Nature* 409, 66 (**2001**).
28. M. S. Gudiksen and C. M. Lieber, *J. Am. Chem. Soc.* 122, 8801 (**2000**).
29. S. Y. Li, P. Lin, C. Y. Lee, and T. Y. Tseng, *J. Appl. Phys.* 95, 3711 (**2004**).
30. S. Y. Li, P. Lin, C. Y. Lee, and T. Y. Tseng, *J. Mater. Sci.: Materials in Electronics* 15, 505 (**2004**).
31. Y. Wu, H. Yan, M. Huang, B. Messer, J. H. Song, and P. Yang, *Chem. Eur. J.* 8, 1261 (**2002**).
32. C. Ma, Y. Ding, D. Moore, X. Wang, and Z. L. Wang, *J. Am. Chem. Soc.* 126, 708 (**2004**).
33. A. Colli, S. Hofmann, A. C. Ferrari, C. Ducati, F. Martelli, S. Rubini, A. Franciosi, and J. Robertson, *Appl. Phys. Lett.* 86, 153103 (**2005**).
34. L. W. Yin, Y. Bando, Y. C. Zhu, and M. S. Li, *Appl. Phys. Lett.* 84, 5314 (**2004**).
35. B. B. Lakshmi, P. K. Dorhout, and C. R. Martin, *Chem. Mater.* 9, 857 (**1997**).
36. (a) K. Rajeswar, N. R. de Tacconi, and C. R. Chenthamarakshan, *Chem. Mater.* 13, 2765 (**2001**); (b) K. Rajeswar, N. R. de Tacconi, and C. R. Chenthamarakshan, *Curr. Opt. Solid State Mater. Sci.* 8, 173 (**2004**).
37. D. Routkevitch, T. Bigioni, M. Moskovits, and J. M. Xu, *J. Phys. Chem.* 100, 14037 (**1996**).
38. D. Xu, X. Shi, G. Guo, L. Gui, and Y. Tang, *J. Phys. Chem. B* 104, 5061 (**2000**).
39. T. Ohgai, L. Gravier, X. Hoffer, and J. P. Ansermet, *J. Appl. Electrochem.* 35, 479 (**2005**).
40. Y. Wang, Z. Y. Tang, X. R. Liang, L. Marz, and N. A. Kotov, *Nano Lett.* 4, 225 (**2004**).
41. Y. Li, Z. Wang, X. D. Ma, X. F. Qian, J. Yin, and Z. K. Zhu, *J. Solid State Chem.* 177, 4386 (**2004**).
42. L. Dloczik, M. C. L. Steiner, and R. Könenkamp, *Thin Solid Films* 431, 131 (**2003**).
43. M. Kaelin, H. Zogg, A. Tiwari, O. Wilhelm, S. E. Pratsinis, T. Meyer, and A. Meyer, *Thin Solid Films* 457, 391 (**2004**).
44. C. Y. Lee, S. Y. Li, P. Lin, and T. Y. Tseng, *J. Nanosci. Nanotech.* 5, 1088 (**2005**).
45. J. A. Voigt, in *Characterization of Ceramics*, edited by R. E. Loehman and L. E. Fitzpatrck, Butterworth-Heinemann, Massachusetts, USA (**1993**).
46. F. H. Chen, H. S. Koo, and T. Y. Tseng, *J. Am. Ceram. Soc.* 75, 96 (**1992**).
47. K. B. Tang, Y. T. Qian, J. H. Zeng, and X. G. Yang, *Adv. Mater.* 15, 448 (**2003**).
48. T. Trindade, P. O' Brien, and N. L. Pickett, *Chem. Mater.* 13, 3843 (**2001**).
49. F. Shieh, A. E. Saunders, and B. A. Korgel, *J. Phys. Chem. B* 109, 8538 (**2005**).
50. Z. A. Peng and X. G. Peng, *J. Am. Chem. Soc.* 124, 3343 (**2002**).
51. L. Manna, E. C. Scher, and A. P. Alivisatos, *J. Cluster Sci.* 13, 521 (**2002**).
52. S. D. Bunge, K. M. Krueger, T. J. Boyle, M. A. Rodriguez, T. J. Headley, and V. L. Colvin, *J. Mater. Chem.* 13, 1705 (**2003**).
53. Z. X. Deng, L. Li, and Y. Li, *Inorg. Chem.* 42, 2331 (**2003**).
54. Y. J. Xiong, Y. Xie, Z. Q. Li, X. X. Li, and S. M. Gao, *Chem. Eur. J.* 10, 654 (**2004**).
55. T. J. Trentler, K. M. Hickman, S. C. Goel, A. M. Viano, P. C. Gibbons, and W. E. Buhro, *Science* 270, 1791 (**1995**).
56. J. Liu, T. Tanaka, K. Sivula, A. P. Alivisatos, and M. J. Fréchet, *J. Am. Chem. Soc.* 126, 6550 (**2004**).
57. W. U. Huynh, J. J. Dittmer, W. C. Libby, G. L. Whiting, and A. P. Alivisatos, *Adv. Funct. Mater.* 13, 73 (**2003**).
58. J. M. Nedeljiković, O. I. Micić, S. P. Ahrenkiel, A. Miedaner, and A. J. Nozik, *J. Am. Chem. Soc.* 126, 2632 (**2004**).
59. E. Arici, N. S. Sariciftci, and D. Meissner, *Adv. Funct. Mater.* 13, 165 (**2003**).
60. S. L. Castro, S. G. Bailey, R. P. Rafaelle, K. K. Banger, S. Fahey, and A. F. Hepp, *Proceedings of 3rd World Conference on Photovoltaic Energy Conversion*, Osaka, Japan (**2003**), p. 2698.
61. H. Grisaru, O. Palchik, A. Gedanken, V. Palchik, M. A. Slifkin, and A. M. Weiss, *Inorg. Chem.* 42, 7148 (**2003**).
62. S. Y. Bae, H. W. Seo, H. C. Choi, J. G. Park, and J. C. Park, *J. Phys. Chem. B* 108, 12318 (**2004**).
63. W. I. Park and G. C. Yi, *Adv. Mater.* 16, 87 (**2004**).
64. G. Yu, J. Gao, J. C. Hummelen, F. Wudl, and A. J. Heeger, *Science* 270, 1789 (**1995**).
65. D. S. Ginger and N. C. Greenham, *Phys. Rev. B* 59, 10622 (**1999**).
66. B. R. Mehta and F. E. Kruis, *Sol. Energy Mater. Solar Cells* 85, 107 (**2005**).
67. A. Hagfeldt and M. Grätzel, *Acc. Chem. Res.* 33, 269 (**2000**).
68. K. Hara, T. Horiguchi, T. Kinoshita, K. Sayama, and H. Arakawa, *Sol. Energy Mater. Solar Cells* 70, 151 (**2001**).
69. K. Hara, T. Nishikawa, M. Kurashige, H. Kawauchi, T. Kashima, K. Sayama, K. Aika, and H. Arakawa, *Sol. Energy Mater. Solar Cells* 85, 21 (**2005**).
70. M. Adachi, Y. Murata, J. Takao, J. Jiu, M. Sakamoto, and F. Wang, *J. Am. Chem. Soc.* 126, 14943 (**2004**).
71. S. Bhattacharya, E. Kymakis, and G. A. J. Amaratunga, *Chem. Mater.* 16, 4819 (**2004**).
72. Y. G. Kim, J. Walker, L. A. Samuelson, and J. Kumar, *Nano Lett.* 3, 523 (**2003**).
73. J. B. Baxter and E. S. Aydil, *Appl. Phys. Lett.* 86, 053114 (**2005**).
74. S. J. Limmer, T. P. Chou, and G. Z. Cao, *J. Mater. Sci.* 39, 895 (**2004**).
75. X. D. Wang, E. Graugnard, J. S. King, Z. L. Wang, and C. J. Summers, *Nano Lett.* 4, 2223 (**2004**).
76. M. Niederberger, M. H. Bartl, and G. D. Stucky, *J. Am. Chem. Soc.* 124, 13642 (**2002**).
77. P. D. Cozzoli, A. Kornowski, and H. Weller, *J. Am. Chem. Soc.* 125, 14539 (**2003**).
78. S. U. M. Khan and T. Sultana, *Sol. Energy Mater. Sol. Cells* 76, 211 (**2003**).
79. S. Liu and K. Huang, *Sol. Energy Mater. Sol. Cells* 85, 125 (**2005**).
80. J. J. Wu and C. C. Yu, *J. Phys. Chem. B* 108, 3377 (**2004**).
81. L. Guo, Y. L. Ji, H. Xu, P. Simon, and Z. Wu, *J. Am. Chem. Soc.* 124, 14864 (**2002**).
82. Y. Lin, D. Wang, Q. Zhao, M. Yang, and Q. Zhang, *J. Phys. Chem. B* 108, 3202 (**2004**).
83. L. Vayssiers, *Adv. Mater.* 15, 464 (**2003**).
84. M. Zheng, G. Li, X. Zhang, S. Huang, Y. Lei, and L. Zhang, *Chem. Mater.* 13, 3859 (**2001**).
85. B. Cheng, J. M. Russel, W. Shi, L. Zhang, and E. T. Samulski, *J. Am. Chem. Soc.* 126, 52 (**2004**).
86. H. Yang, Q. Shi, B. Tian, Q. Lu, F. Gao, S. Xie, J. Fan, C. Yu, B. Tu, and D. Zhao, *J. Am. Chem. Soc.* 125, 4724 (**2003**).
87. T. Lindgren, H. Wang, N. Beermann, L. Vayssiers, A. Hagfeldt, and S. E. Linquist, *Sol. Energy Mater Sol. Cells* 71, 231 (**2002**).
88. X. Wang, X. Chen, L. Gao, H. Zheng, Z. Zhang, and Y. Qian, *J. Phys. Chem. B* 108, 16401 (**2004**).
89. G. Malandrino, S. T. Finocchiaro, R. L. Nigro, C. Bongiorno, C. Spinella, and I. L. Fragalà, *Chem. Mater.* 16, 5559 (**2004**).
90. C. J. Brabec, *Sol. Energy Mater. Solar Cells* 83, 273 (**2004**).

91. H. Spanggaard and F. C. Krebs, *Sol. Energy Mater. Solar Cells* 83, 125 (**2004**).
92. C. W. Tang, *Appl. Phys. Lett.* 48, 183 (**1986**).
93. F. Yang, M. Shtein, and S. R. Forrest, *Nature Mater.* 4, 37 (**2005**).
94. K. M. Coakley and M. D. McGehee, *Chem. Mater.* 16, 4533 (**2004**).
95. A. P. Smith, R. P. Smith, B. E. Taylor, and M. F. Durstock, *Chem. Mater.* 16, 4687 (**2004**).
96. S. E. Shaheen, C. J. Brabec, and N. S. Sariciftci, *Appl. Phys. Lett.* 78, 841 (**2001**).
97. J. F. Nierengarten, *Sol. Energy Mater. Solar Cells* 83, 187 (**2004**).
98. C. Yang, H. Li, Q. Sun, J. Qiao, Y. Li, Y. F. Li, and D. Zhu, *Sol. Energy Mater. Solar Cells* 85, 241 (**2005**).
99. B. Pradhan and A. J. Pal, *Sol. Energy Mater. Solar Cells* 81, 469 (**2004**).
100. K. Takahashi, T. Kuraya, T. Yamaguchi, T. Komura, and K. Murata, *Sol. Energy Mater. Solar Cells* 61, 403 (**2000**).
101. J. C. Bernede, H. Derouiche, and V. Djara, *Sol. Energy Mater. Solar Cells* 87, 261 (**2005**).
102. J. Rostalski and D. Meissner, *Sol. Energy Mater. Solar Cells* 61, 87 (**2000**).
103. C. Videlot, A. E. Kassmi, and D. Fichou, *Sol. Energy Mater. Solar Cells* 63, 69 (**2000**).
104. D. Gebeyehu, B. Maennig, J. Drechsel, K. Leo, and M. Pfeiffer, *Sol. Energy Mater. Solar Cells* 79, 81 (**2003**).
105. F. Nüsch, G. Tornare, L. Zuppiroli, F. Meng, K. Chen, and H. Tian, *Sol. Energy Mater. Solar Cells* 87, 817 (**2005**).
106. J. J. Dittmer, R. Lazzaroni, Ph. Leclère, P. Moretti, M. Granström, K. Petrisch, E. A. Marseglia, R. H. Friend, J. L. Bredas, H. Rost, and A. B. Holmes, *Sol. Energy Mater. Solar Cells* 61, 53 (**2000**).

Received: 5 July 2005. Revised/Accepted: 25 July 2005.